Received: 11 July 2023 | Revised: 22 September 2023 | Accepted: 5 October 2023

DOI: 10.1002/aic.18285

RESEARCH ARTICLE

Process Systems Engineering

AIChE JOURNAL

Model-based design of stratified packings for enhanced mass transfer using optimal control theory

A. Eppink | M. Kuhn | H. Briesen

Technical University of Munich, Process Systems Engineering, Freising, Germany

Correspondence
H. Briesen, Technical University of Munich, Process Systems Engineering, Gregor-Mendel-Straße 4, 85354 Freising, Germany.
Email: heiko.briesen@tum.de

Funding information
Deutsche Forschungsgemeinschaft, Grant/Award Number: 493700036

Abstract

Various examples show that stratified columns can improve the transport performance of particle packings. However, to date, there is no universal strategy to design these packings to yield optimal performance. This study proposes a model-based approach for designing particle packings in which mass transfer occurs between a liquid phase and a stationary phase using optimal control theory. The primary objective is to provide a general design strategy that is applicable across different unit operations in chemical, pharmaceutical, and food applications. Optimal control is utilized to determine the optimal particle diameter as a function of the axial position within the column. We demonstrate the approach using two case studies and three different optimization criteria. Numerical results indicate that the proposed method is highly effective, for example, the solvent demand is reduced by up to 32.47%. Moreover, the optimally graded packing yields a significantly sharper breakthrough curve of an adsorption column.

KEYWORDS
model-based design, numerical modeling, optimal control theory, stratified particle columns, transport processes

1 | INTRODUCTION

Diffusive mass transfer between a stationary phase and a liquid phase, as well as various adsorption processes, exist in many different industries, including the pharmaceutical, chemical, and food industries. Chromatographic separation processes,[1,2] adsorption columns,[3–5] coffee extraction,[6,7] and porous media washing[8] are exemplary applications. These processes typically involve homogeneous packings with a constant mean particle diameter along the axial direction.

Several studies show that packings with a gradient of the particle diameter could have beneficial properties. Pota and Mathews[9] passed a flow through a stratified fixed bed adsorber in both directions and found that the breakthrough curves were not identical. Better results were achieved with decreasing particle diameters in the axial direction. Naidu and Mathews[10] obtained sharper breakthrough curves using stratified adsorption columns for the separation of bioproduced acetic acid. Li and Liapis[11] investigated layered adsorption columns and concluded that decreasing particle diameters in the axial direction lead to longer breakthrough times, and, thus, could be particularly advantageous for high flow rates. Sze and McKay[12] mitigated para-chlorophenol through stratified activated carbon adsorption columns. Hernández-Hernández et al.[13] found that stratified adsorption columns have better breakthrough parameters than conventional packed beds for the binary adsorption of heavy metals. Bruttini and Liapis[14] accelerated the drying rates of a freeze-drying system using stratified packings. Besides these observational studies, only a few studies have considered the actual stratification design. Salloum and Robinson[15]

optimized the flow through porous particle packings by spatially varying the permeability. Georgiadis and Kostoglou[16] developed multilaminated polymer matrix devices using optimal control to enable controlled drug release. Kuhn et al.[17] addressed the methodological gap in depth filtration by designing layered depth filters using optimal control theory. Kuhn and Briesen[18] applied the same methodology to the axial resistance profile of submerged hollow membranes. In addition to the beneficial properties of stratified columns, 3D printing has increased the possibilities of manufacturing such packings, allowing enhanced freedom of design.[19–21]

Various approaches can be used to model the transport processes in porous beds. Typically, continuum models[22–24] or discrete pore-scale models[25,26] are used. The optimal design strategy requires reasonable computational effort, so we opt for the 1D transport dispersive model at the continuum level. Our approach addresses transport processes in porous media, where diffusive mass transfer between the pore phase and the fluid phase is the rate-limiting step. Additionally, molecules adsorb onto the surfaces of the porous stationary phase. We consider the two mass transfer cases separately: mass transfer from the stationary phase into the fluid phase (Case A) and mass transfer from the fluid phase into the stationary phase (Case B). For both cases, various applications exist. Examples of Case A are washing of porous media, such as filter cake washing, coffee extraction, or removing impurities in porous solids.[6,8,27,28] In Case B, the mass transfer occurs in the opposite direction. Initially, an unloaded stationary phase is flowed by a fluid phase containing a target component to load the solid phase with this target component or to remove the target component from the liquid phase.[29–31]

The approach presented has a high degree of generality from utilizing the classical continuum approach combined with established constitutive relationships. Furthermore, well-established parametrization strategies are available. Though no experimental data is investigated here, the used model and correlations are already widely validated and frequently used to describe transport processes in porous media. Instead, we present a model-based approach using optimal control for designing columns with a particle diameter as a function of the axial variable.

2 | CASE STUDIES

We demonstrate our methodology using two case studies A and B combined with three optimization criteria corresponding to three objective functionals J_1, J_2, and J_3. In both cases, we consider a fluid phase flowing through a porous stationary phase and examine the mass transfer of a target component in the fluid and between the fluid phase and the solid phase. Consequently, the transport phenomena we investigate are convection, dispersion, molecular diffusion, and adsorption. The transfer of our approach to other applications with similar transport processes such as chromatographic separation should be straightforward.

2.1 | Case A: Solid–liquid extraction

In Case A, the mass transfer from the solid phase into the liquid phase is optimized. The stationary phase is initially loaded with a target component, and a solvent extracts such component into the liquid phase (Figure 1, left). The blue color scale illustrates the concentration in the porous particles of the stationary phase. The darker the blue, the higher the corresponding concentration. At time $t = 0$, the mobile phase is filled with an inert fluid into which the target component does not diffuse. Extraction from the stationary phase only occurs when it gets into contact with the solvent (Figure 1, middle). The molecules of the target component desorb from the solid surfaces into the pore phase of the porous particles and diffuse into the mobile phase. At entry, the column is flowed through with pure solvent. Consequently, a phase boundary between the inert phase and the solvent phase must be implemented, which passes through the packing at the beginning of the process. At finite time $t = t^{end}$, the process is finished. The decreasing concentration difference between the mobile phase and the stationary phase in axial direction z, results in an inhomogeneous washing for a packing with constant particle diameter (Figure 1, right).

2.2 | Case B: Adsorption columns

In Case B, we examine the scenario of opposite mass transfer, which involves the diffusion and adsorption of a target component into a porous stationary phase. Specifically, we consider a system where the target component is initially not present in the mobile phase or in the stationary phase (Figure 2, left). At entry, the target component is dissolved in the fluid inlet stream. As the mobile phase passes through the packing, the molecules of the target component diffuse into the porous particles and adsorb onto the surfaces of the solid phase (Figure 2, middle). As in Case A, for a homogeneous packing with constant particle diameter, an inhomogeneous loading of the stationary phase is obtained if the process is terminated at finite time $t = t^{end}$ (Figure 2, right).

3 | MODEL-BASED APPROACH

3.1 | Modeling

To design graded particle columns using optimal control theory, a mathematical model must represent the relevant physical phenomena of Case A and B. As both cases reflect the same physical phenomena, their distinction is done only via the boundary conditions and initial conditions in Section 3.2. First, a mass balance of the target component in the mobile phase and the stationary phase is formulated. The transport dispersive model is used to describe the mass transfer in porous particle packings assuming an isothermal process. For detailed information regarding the transport dispersive model, the reader is

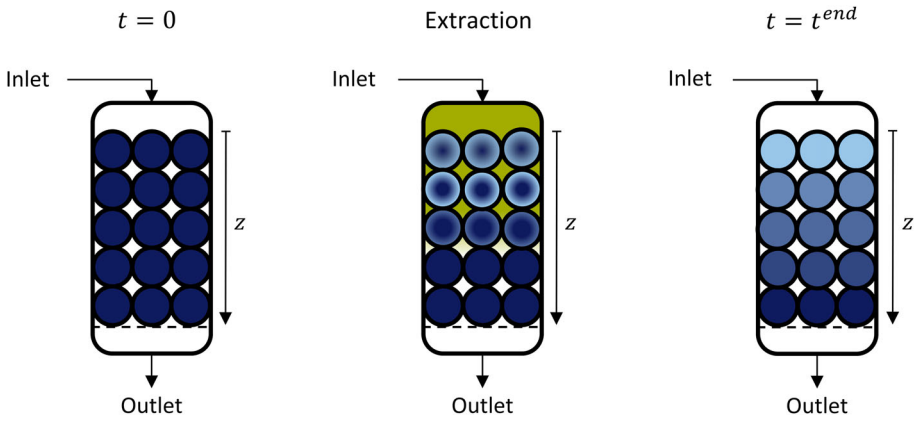

FIGURE 1 In Case A at $t = 0$, the porous particles contain the target component. Through flushing the packing with the solvent, the target component desorbs into the pore phase and diffuses into the mobile phase.

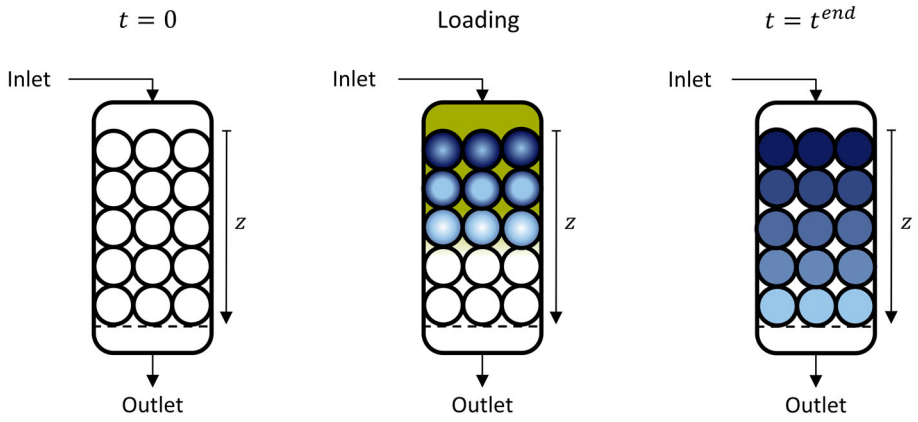

FIGURE 2 In Case B at $t = 0$, the target component is neither present in the stationary phase nor the mobile phase. Through flushing the packing with an inlet stream containing the target component, the target component diffuses into the pore phase and adsorbs onto the surfaces of the porous particles.

referred to, for example, Schmidt-Traub et al.[32] The model comprises the mass balance of the target compound in the fluid phase:

$$\frac{\partial c}{\partial t} = -\frac{v}{\varepsilon}\frac{\partial c}{\partial z} + D_{ax}\frac{\partial^2 c}{\partial z^2} - \frac{1-\varepsilon}{\varepsilon}\frac{\partial c_{stat}}{\partial t}, \tag{1}$$

c is the fluid phase concentration of the target component; ε is the bed porosity; t is the time variable; z is the axial variable; D_{ax} is the axial dispersion coefficient; c_{stat} is the stationary phase concentration of the target component; v is the superficial velocity. Additionally, a second mass balance is formulated for the domain of the porous stationary phase c_{stat}, which changes only due to diffusive mass transfer between the pore phase and the liquid phase. Since the stationary phase consists of porous particles, the stationary phase comprises the pore phase and the solid phase.

$$\frac{\partial c_{stat}}{\partial t} = k_{eff}(c - c_p)\frac{6}{d_p}, \tag{2}$$

k_{eff} is the effective mass transfer coefficient; c_p is the concentration of the target compound in the liquid pore particle phase; d_p is the particle diameter. The driving force of mass transfer is the concentration difference between the liquid phase and the pore phase $(c - c_p)$. The diffusive mass transfer across the liquid boundary layer and the intra-particle diffusive mass transfer are considered to be rate-limiting. The effective mass transfer coefficient k_{eff} combines these two effects. All parameters must be formulated as a function of the particle diameter d_p to implement the optimal control problem. For the description of the film mass transfer coefficient k_{film}, the correlation according to Wilson and Geankoplis,[33] and for the pore mass transfer coefficient k_{pore}, the correlation according to Mackie and Meares[34] are used:

$$\frac{1}{k_{eff}} = \frac{1}{k_{film}} + \frac{1}{k_{pore}}, \tag{3}$$

$$k_{film} = \frac{1.09}{\varepsilon}\frac{D_m}{d_p}\left(\frac{v \cdot d_p}{D_m}\right)^{0.33}, \tag{4}$$

$$k_{pore} = \frac{10}{d_p}\frac{\varepsilon_p^2}{(2-\varepsilon_p)^2}D_m, \tag{5}$$

ε_p is the inner-particle porosity; D_m is the molecular diffusion coefficient in the liquid phase. In addition to intra-particle diffusion, the molecules adsorb and desorb onto the porous particle surfaces. As common in many processes, adsorption and desorption rates are assumed to be significantly faster than diffusive phenomena.[32] Therefore, the equilibrium between the solid phase and the pore phase is instantaneously present and is described through the Langmuir adsorption isotherm:

$$c_s = \frac{a \cdot c_p}{1 + b \cdot c_p}, \tag{6}$$

c_s is the concentration in the solid phase of the particles; a and b are parameters of the Langmuir adsorption isotherm. A closing condition between the concentrations within the stationary phase is finally formulated, connecting the concentrations in the pore space c_p, the solid phase c_s, and the overall stationary phase domain c_{stat} via the particle porosity ε_p:

$$c_{stat} = \varepsilon_p \cdot c_p + (1 - \varepsilon_p) c_s. \tag{7}$$

Besides the mass transfer between the stationary phase and the liquid phase and convection, molecular diffusion and axial dispersion occur in the liquid phase. These two effects are summarized by the axial dispersion coefficient D_{ax} (Equation 8), which is estimated according to the correlation of Chung and Wen.[35] The pressure drop Δp across a particle packing is determined using the integrated form of a localized Kozeny–Carman Equation (9)[36,37]:

$$D_{ax} = \frac{v \cdot d_p}{0.2 + 0.011 \left(\frac{v \cdot d_p \cdot \rho}{\eta}\right)^{0.48}}, \tag{8}$$

$$\Delta p = \int_0^L k_0 \frac{(1-\varepsilon)^2}{\varepsilon^3} \frac{\eta \cdot v}{d_p^2} dz, \tag{9}$$

ρ is the density of the fluid; η is the dynamic viscosity of the fluid; k_0 is an unknown factor depending on the structure of the packed bed; L is the length of the column.

Since the main objective of this article is to develop a general method, we use a non-dimensionalized form of the model. The non-dimensionalized model also provides advantages in numerical optimization due to the implicit scaling. The detailed derivation of the non-dimensional model in Equations (10)–(16) is given in the Supplementary Material.

$$\frac{\partial \tilde{c}}{\partial \tilde{t}} = -\frac{\partial \tilde{c}}{\partial \tilde{z}} + \frac{1}{Bo\left(\tilde{d}_p\right)} \frac{\partial^2 \tilde{c}}{\partial \tilde{z}^2} - \frac{1-\varepsilon}{\varepsilon} \frac{\partial \tilde{c}_{stat}}{\partial \tilde{t}}, \tag{10}$$

$$\frac{\partial \tilde{c}_{stat}}{\partial \tilde{t}} = St_{mod}\left(\tilde{d}_p\right)(\tilde{c} - \tilde{c}_p), \tag{11}$$

$$\tilde{c}_s = \frac{a \cdot \tilde{c}_p}{1 + b \cdot \tilde{c}_p \cdot c^0}, \tag{12}$$

$$\tilde{c}_{stat} = \varepsilon_p \cdot \tilde{c}_p + (1 - \varepsilon_p)\tilde{c}_s, \tag{13}$$

$$\Delta \tilde{p} = \int_0^1 \frac{1}{\tilde{d}_p^2} d\tilde{z}, \tag{14}$$

$$Bo\left(\tilde{d}_p\right) = \tilde{a} \cdot \frac{0.2 + \tilde{b} \cdot \tilde{d}_p^{0.48}}{\tilde{d}_p}, \tag{15}$$

$$St_{Mod}\left(\tilde{d}_p\right) = \frac{\tilde{c}}{\frac{\tilde{d}_p^{1.67}}{\tilde{d}} + \frac{\tilde{d}_p^2}{\tilde{e}}}, \tag{16}$$

Bo is the Bodenstein number; St_{mod} is the modified Stanton number; c^0 is the basis concentration; $\tilde{a}, \tilde{b}, \tilde{c}, \tilde{d}$ and $\tilde{e}$ are the non-dimensional model parameters (Supplementary Material). Note the many dependencies of Equations (15) and (16) on the particle size $\tilde{d}_p$. In homogeneous packings, these values would be fixed. And of course, the performance depends on that fixed particle size $\tilde{d}_p$. However, here we are explicitly searching for a stratified column with a spatially dependent particle size $\tilde{d}_p(\tilde{z})$ to optimize process performance.

3.2 | Initial conditions and boundary conditions

3.2.1 | Initial conditions and boundary conditions for Case A

In order to model Case A, the initial and boundary conditions need to be defined. As mentioned in Section 2.1, the target component is in the stationary phase at the beginning, and the column is flushed with pure solvent. The outlet of the column is implemented as a constant flux. Mathematically formulated, the initial conditions in Equations (17) and (18) and the boundary conditions in Equations (19) and (20) are obtained:

$$\tilde{c}\left(\tilde{t} = 0, \tilde{z}\right) = 0 \ \forall \ \tilde{z} \in [0,1], \tag{17}$$

$$\tilde{c}_{stat}\left(\tilde{t} = 0, \tilde{z}\right) = 1 \ \forall \ \tilde{z} \in [0,1], \tag{18}$$

$$\tilde{c}\left(\tilde{t}, \tilde{z} = 0\right) = 0, \tag{19}$$

$$\frac{\partial \tilde{c}\left(\tilde{t}, \tilde{z} = 1\right)}{\partial \tilde{z}} = 0. \tag{20}$$

3.2.2 | Initial conditions and boundary conditions for Case B

In Case B, at $\tilde{t} = 0$, the target component is neither in the mobile phase nor the stationary phase. Instead, an inlet stream where the target component is dissolved flows through the column (Section 2.2). Mathematically, the initial conditions are given in Equations (21) and (22), and the boundary conditions in Equations (23) and (24).

$$\tilde{c}\left(\tilde{t} = 0, \tilde{z}\right) = 0 \ \forall \ \tilde{z} \in [0,1], \tag{21}$$

$$\tilde{c}_{stat}\left(\tilde{t} = 0, \tilde{z}\right) = 0 \ \forall \ \tilde{z} \in [0,1], \tag{22}$$

$$\tilde{c}\left(\tilde{t}, \tilde{z} = 0\right) = 1, \tag{23}$$

TABLE 1 Numerical parameters for objectives J_1 and J_2 for both Case A and Case B.

Parameter	Value
$\tilde{a}$	11,905
$\tilde{b}$	2.985×10^{-2}
$\tilde{c}$	12,600
$\tilde{d}$	1.346×10^{-3}
$\tilde{e}$	2.6×10^{-5}
a	10
b	0.009
c^0	100 $\left[\frac{\text{kg}}{\text{m}^3}\right]$
d_p^0	1×10^{-4} [m]
$\tilde{d}_p^{min}$	0.3
$\tilde{d}_p^{max}$	1
$\tilde{t}^{end}$	4
$\tilde{c}_{stat}^{tar}$	0.3/1.4
$\tilde{p}^{max}$	2.367

$$\frac{\partial \tilde{c}(\tilde{t},\tilde{z}=1)}{\partial \tilde{z}} = 0. \tag{24}$$

3.2.3 | Choice of parameters

For the optimization problems corresponding to the functionals J_1 and J_2 (to be defined in Section 3.3), the same values of the model parameter are chosen for Case A and Case B (see Section 2). This case study is not based on any particular experiment, but is a theoretical consideration of various possible applications. Nevertheless, all parameters are chosen in a realistic range (Table 1). Furthermore, the ratio between convection and diffusive mass transport is decisive for objectives J_1 and J_2, which is proportional to the volumetric flow rate and, thus, can be controlled.

For the optimization of the objective functional J_3, we only consider Case B and are guided by the paper by Naidu and Mathews.[10] There, a significantly sharper breakthrough curve was achieved by stratifying an adsorption column with activated carbon for the separation of bioproduced acetic acid. We use the same material parameters in this work. However, the model and the correlations used in Naidu and Mathews[10] differ from those in our proposed method. Naidu and Mathews[10] created a stratified packing consisting of five distinct layers. The mean particle diameters of the individual layers decreased in the axial direction. This stratified column is the benchmark for the resulting optimal profile of the particle diameter $\tilde{d}_p$. $\tilde{d}_p^1 - \tilde{d}_p^5$ are the mean particle diameters of the five layers from Naidu and Mathews.[10] We obtain as an optimal solution a function of the particle diameter $\tilde{d}_p$ of the axial variable $\tilde{z}$. We approximate this optimal function with a constant piecewise function to determine five optimal layers. The column consisting of those five layers has the same pressure drop $\Delta\tilde{p}$ as the optimal column. Table 2 shows all relevant model parameters for objective functional J_3.

TABLE 2 Numerical parameters for objective J_3 for Case B.

Parameter	Value
$\tilde{a}$	352.05
$\tilde{b}$	7.978×10^{-3}
$\tilde{c}$	403.385
$\tilde{d}$	4.044×10^{-2}
$\tilde{e}$	5.402×10^{-3}
a	209.41
b	0.53
c^0	17.7 $\left[\frac{\text{kg}}{\text{m}^3}\right]$
d_p^0	1.3×10^{-3} [m]
$\tilde{d}_p^{min}$	0.1
$\tilde{d}_p^{max}$	1
$\tilde{t}^{end}$	15
$\tilde{p}^{max}$	4.522
$\tilde{d}_p^1;\tilde{d}_p^2;\tilde{d}_p^3;\tilde{d}_p^4;\tilde{d}_p^5$	0.705;0.593;0.498;0.419;0.352

3.3 | Optimization criteria

3.3.1 | Maximize mass transfer

Optimization criteria for optimal control problems are formulated in terms of functionals. The first objective functional considered is the maximum mass transfer J_1. In Case A, examples of objective J_1 are solid–liquid extraction processes such as espresso preparation. The goal is to extract the maximum of a target component from a given amount of ground coffee. In Case B, a possible application of the objective functional J_1 is the removal of a target component from a liquid phase. The minimum amount of the target component should leave the column at the outlet. Therefore, at a maximum mass transfer, the time integration of the breakthrough concentration $\tilde{c}(\tilde{t},\tilde{z}=1)$ becomes maximal in Case A or minimal in Case B if a constant superficial velocity is considered. Without formulating a constraint, the optimizer would deliver a homogeneous packing with minimum particle diameter $\tilde{d}_p$ to maximize surface area over the entire axial position $\tilde{z}$ as a solution. However, such packing would be associated with a huge pressure drop $\Delta\tilde{p}$. For this reason, a maximum allowable pressure drop $\Delta\tilde{p}^{max}$ over the column is formulated as a constraint. Moreover, we define a minimal particle diameter $\tilde{d}_p^{min}$ and a maximal particle diameter $\tilde{d}_p^{max}$, which would reflect natural limitations on available particle sizes $\tilde{d}_p$:

$$\min J_1 = \pm \int_0^{\tilde{t}^{end}} \tilde{c}(\tilde{t},\tilde{z}=1)\, d\tilde{t}, \tag{25}$$

$$s.t.\ \text{Equations}\,(10)-(16), \tag{26}$$

$$\Delta\tilde{p} \le \Delta\tilde{p}^{max}, \tag{27}$$

$$\tilde{d}_p \ge \tilde{d}_p^{min} \ \ \forall\ \tilde{z} \in [0,1], \tag{28}$$

$$\tilde{d}_p \le \tilde{d}_p^{max} \ \ \forall\ \tilde{z} \in [0,1]. \tag{29}$$

3.3.2 | Minimize solvent demand

The second objective functional is the minimum solvent demand J_2. Objective J_2 for Case A represents the removal of impurities in a stationary phase by flushing the column with a solvent. Considering the objective functional J_2 for Case B is a theoretical case study with no direct application. The process is finished if the concentration in the stationary phase falls below (Case A) or exceeds (Case B) a defined target concentration $\tilde{c}_{stat}^{tar}$ along the entire axial position $\tilde{z}$. The solvent demand $\tilde{V}_{Solvent}$ is minimized until the process ends. Since the volumetric flow rate, bed porosity ε, and inner column diameter are constant, the solvent demand is proportional to the time needed to reach the target concentration in the stationary phase: $\tilde{V}_{Solvent} \propto \tilde{t}^{end}$. Similar as for objective J_1, the maximum pressure drop $\Delta\tilde{p}^{max}$ again is formulated as a constraint because a homogeneous packing with minimum particle diameter $\tilde{d}_p^{min}$ would again be the trivial optimal solution for unconstrained pressure drop $\Delta\tilde{p}$:

$$\min J_2 = \tilde{V}_{Solvent}, \tag{30}$$

$$s.t.\ \text{Equations}\,(10)-(16), \tag{31}$$

$$\Delta\tilde{p} \le \Delta\tilde{p}^{max}, \tag{32}$$

$$\tilde{d}_p \ge \tilde{d}_p^{min} \ \ \forall\ \tilde{z} \in [0,1], \tag{33}$$

$$\tilde{d}_p \le \tilde{d}_p^{max} \ \ \forall\ \tilde{z} \in [0,1], \tag{34}$$

$$\pm\tilde{c}_{stat}\left(\tilde{t}=\tilde{t}^{end},\tilde{z}\right) \le \pm\tilde{c}_{stat}^{tar} \ \ \forall\ \tilde{z} \in [0,1]. \tag{35}$$

3.3.3 | Sharp breakthrough curve

For the final objective J_3, we consider only Case B. The breakthrough curve of an ideal adsorption column would elute exactly like the inlet concentration profile, only delayed due to the diffusive mass transfer and adsorption processes. Accordingly, the theoretically ideal sharp breakthrough curve $\tilde{c}^{sharp}$ would have a vertical edge in Case B (Figure 8). The objective J_3 aims to minimize the difference between the breakthrough curve of the optimal packing and the theoretically ideal breakthrough curve $\tilde{c}^{sharp}$. Note that this theoretically ideal sharp breakthrough curve $\tilde{c}^{sharp}$ cannot be reached in reality and in the used model due to non-ideal effects such as molecular diffusion, axial dispersion, and mass transfer between the stationary phase and the liquid phase. The assessment of the remaining deviation from that ideal state is done by evaluating the L_2-norm of the difference function in the time domain. Again, the maximum pressure drop $\Delta\tilde{p}^{max}$ is used as a constraint to achieve comparability between the optimal column and the homogeneous column:

$$\min J_3 = \int_0^1 \left[\tilde{c}\left(\tilde{t},\tilde{z}=1\right) - \tilde{c}^{sharp}\right]^2 d\tilde{t}, \tag{36}$$

$$s.t.\ \text{Equations}\,(10)-(16), \tag{37}$$

$$\Delta\tilde{p} \le \Delta\tilde{p}^{max}, \tag{38}$$

$$\tilde{d}_p \ge \tilde{d}_p^{min} \ \ \forall\ \tilde{z} \in [0,1], \tag{39}$$

$$\tilde{d}_p \le \tilde{d}_p^{max} \ \ \forall\ \tilde{z} \in [0,1]. \tag{40}$$

3.4 | Numerical solution

The two coupled partial differential equations (PDEs) in Equations (10) and (11) are solved using the method of lines. First, the spatial direction is discretized using 200 equidistantly distributed discretization points. Then, first-order partial derivatives are approximated using a five-point upwind scheme, and second-order partial derivatives are approximated using a three-point central scheme. The Van Leer flux limiter is implemented to prevent oscillations in areas of steep moving fronts.[38] In our model, a steep moving front exists in Case A at the phase boundary between the solvent phase and the inert phase, and in Case B the moving solute front. Finally, the resulting system of ordinary equations (ODEs) is solved with the implicit time integration scheme ode15s in MATLAB (Version R2023a, supplier: The MathWorks, Natick, Massachusetts).

We use an optimal control approach to find an optimal continuous function of the particle diameter rather than optimal discrete layers as in standard optimization techniques. The optimal control problem is reduced to a conventional optimization problem by combining control parametrization with a direct-single-shooting method.[38,39] In Figure 3, the blue line is the optimal function of the particle diameter $\tilde{d}_p$. This function is naturally not known in optimal control problems. First, the particle diameter $\tilde{d}_p$ is assumed to be a linear function of the axial variable $\tilde{z}$. Therefore, the particle diameters $\tilde{d}_p$ at the inlet and outlet are optimally determined with all diameters

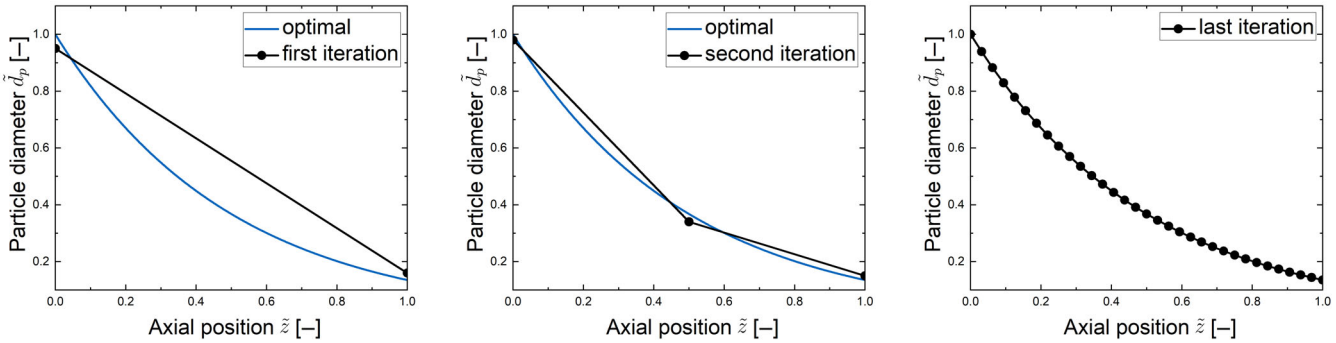

FIGURE 3 Illustration of the numerical solution strategy to solve the optimal control problems by combining control parametrization with a direct-single-shooting method.[38,39]

at each axial discretization point linearly interpolated between those two points (Figure 3, left). In the second iteration, a third control point is added in the middle of the two points of the first iteration. The three control variables are again determined optimally with continuous information along the axis $\tilde{z}$ being linearly interpolated between the points (Figure 3, middle). Before each iteration, the control variables are initialized with the values of the previous iteration to increase speed and robustness of the optimization algorithm. With each iteration, one point is added between every two points. Using this successive refinement strategy, theoretically any continuous function can be approximated, including strongly non-linear functions, if enough iterations are performed (Figure 3, right).[17,39] In this work, a total of five iterations and thus 17 points are used to obtain the optimal function of the particle diameter $\tilde{d}_p$. fmincon, a numerical gradient-based solver in MATLAB, is used to solve the optimization problems.

4 | RESULTS AND DISCUSSION

4.1 | Maximize mass transfer

First, we investigate the results for maximizing the mass transfer J_1. For both Case A and Case B, the optimal solution is actually a homogeneous packing with constant particle diameter $\tilde{d}_p$ as shown in Figure 4. The optimal control formulation cannot achieve any particular improvement. The constant particle diameter $\tilde{d}_p$ maximizes the specific surface area and intra-particle diffusion rates over the complete column if the pressure drop $\Delta\tilde{p}$ is formulated as a constraint (Table 3). Thus, the homogeneous column maximizes the overall diffusive mass transfer between the liquid phase and the stationary phase. In this case, particles are washed out (Case A) or loaded (Case B) faster at the column's inlet than at the column's outlet since the concentration difference between the mobile phase and the stationary phase decreases in the axial direction $\tilde{z}$ (Figure 4). Note that it may be possible to achieve minor improvements in other parameter ranges. We have focused on a realistic range for the model parameters in which the homogeneous packing is optimal. While not providing a particularly exciting solution, these cases still show that the overall strategy also retrieves the potentially simple solutions.

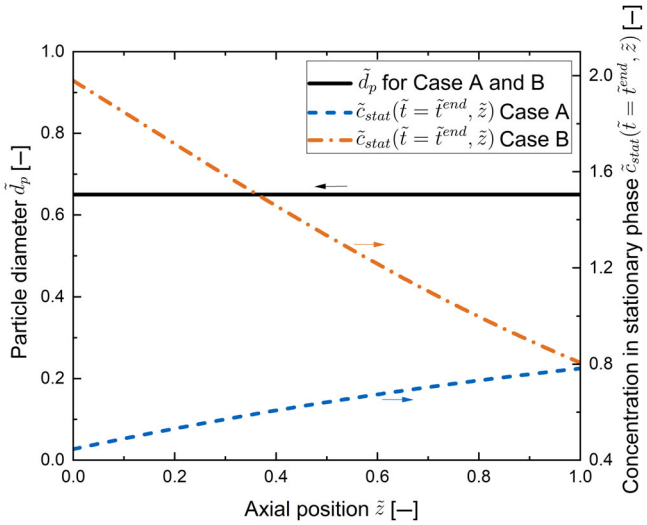

FIGURE 4 Resulting optimal particle diameter $\tilde{d}_p$ for objective J_1 for Case A and Case B and the concentration in the stationary phase at the end of the process $\tilde{c}_{stat}$ over the axial position $\tilde{z}$.

TABLE 3 Averaged modified Stanton number St_{mod} over the complete column and the solvent demand $\tilde{V}_{Solvent}$ for the homogeneous packing (optimal for J_1) and the two optimal profiles $\tilde{d}_p$ (optimal for Case A and Case B for J_2).

Packing	St_{mod}	$\tilde{V}_{Solvent}$
Optimal $\tilde{d}_p$ for J_1 Case A and Case B	0.77086	1
Optimal $\tilde{d}_p$ for J_2 Case A	0.77063	0.7541
Optimal $\tilde{d}_p$ for J_2 Case B	0.77057	0.6753

4.2 | Minimize solvent demand

The second objective J_2 aims to minimize the solvent demand $\tilde{V}_{Solvent}$ until the concentration in the stationary phase falls below (Case A) or reaches (Case B) the defined target concentration $\tilde{c}_{stat}^{tar}$ at every axial position $\tilde{z}$. The resulting optimal particle diameters $\tilde{d}_p$ as functions of

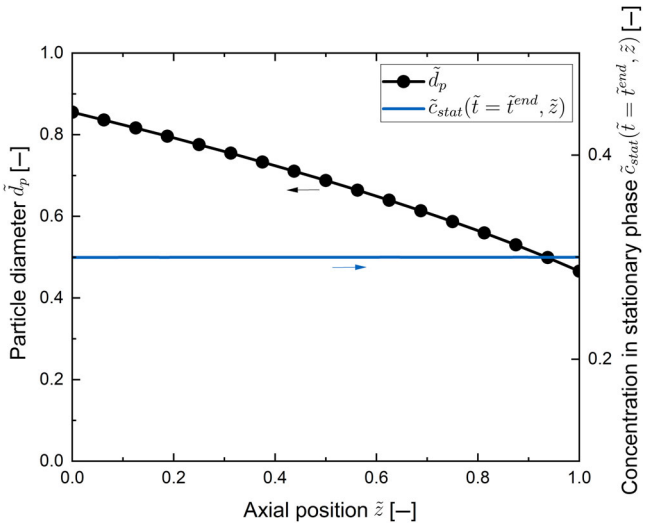

FIGURE 5 Resulting optimal particle diameter $\tilde{d}_p$ for objective J_2 for Case A and the concentration in the stationary phase at the end of the process $\tilde{c}_{stat}$ over the axial position $\tilde{z}$.

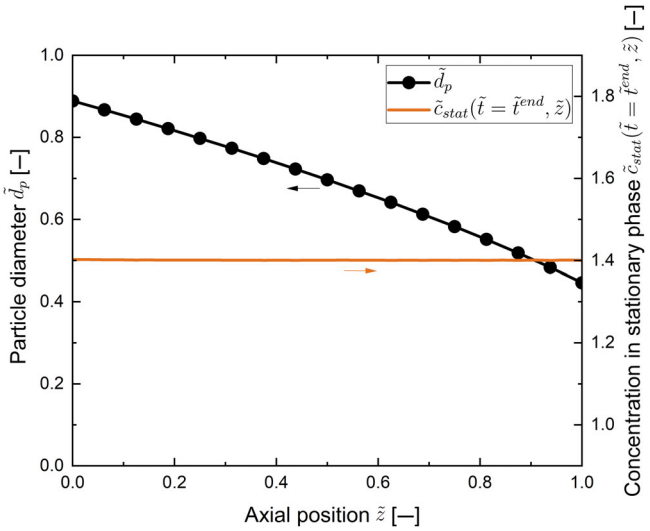

FIGURE 6 Resulting optimal particle diameter $\tilde{d}_p$ for objective J_2 for Case B and the concentration in the stationary phase at the end of the process $\tilde{c}_{stat}$ over the axial position $\tilde{z}$.

the axial position $\tilde{z}$ are illustrated in Figure 5 for Case A and in Figure 6 for Case B. The mass transfer is homogenized in both cases as the particle diameter $\tilde{d}_p$ decreases along the axial position $\tilde{z}$. The decreasing concentration difference in the axial direction $\tilde{z}$ between the mobile phase and the pore phase is compensated by the increasing specific surface area and the faster intra-particle diffusion of the smaller particles. This results in a homogeneous washing (Case A, Figure 5) or loading (Case B, Figure 6), and, thus, the target concentration $\tilde{c}_{stat}^{tar}$ is reached simultaneously along the column in axial direction $\tilde{z}$ at the end of the process $\tilde{t}^{end}$.

In Table 3, the average modified Stanton number St_{mod} over the axial position $\tilde{z}$ and the solvent demand $\tilde{V}_{Solvent}$ are shown for the homogeneous packing (optimal for J_1) and the two optimal profiles of $\tilde{d}_p$ (optimal for J_2). The modified Stanton number St_{mod} relates convection and diffusive transport between the liquid phase and the pore phase. The higher the modified Stanton number St_{mod}, the higher the diffusive mass transfer between liquid and pore phases in relation to convection. The homogeneous column has a slightly higher averaged modified Stanton number St_{mod} compared to the stratified packings. For this reason, the overall mass transfer is maximized, and the homogeneous packing is optimal for objective J_1. However, the averaged modified Stanton number St_{mod} is only minimally lower for the two packings with gradients of particle diameter $\tilde{d}_p$ and, thus, the overall mass transfer is only slightly lower. If the homogeneous packing is used, the mass transfer between the liquid phase and the stationary phase is faster at the inlet of the column and decreases along the axial position $\tilde{z}$ due to the decreasing concentration difference. The result is an inhomogeneous washing/loading of the solid phase (Figure 4). Since the optimally stratified packing allows this homogeneous mass transfer with only a slightly lower overall modified Stanton number St_{mod} and thus only slightly lower overall mass transfer, significantly less solvent is needed to reach the target concentration $\tilde{c}_{stat}^{tar}$ along the entire column in axial direction $\tilde{z}$ (Table 3). In Case A, a reduction in solvent demand $\tilde{V}_{Solvent}$ of 24.59% compared to the homogeneous packing is achieved. In Case B, the optimal packing reduces the solvent demand $\tilde{V}_{Solvent}$ by 32.47% (Table 3).

It is important to mention that the perfect homogeneous washing (Case A) or loading (Case B) as illustrated in Figures 5 and 6 is only possible if convection and diffusive mass transfer between the liquid phase and the solid phase are in a certain ratio. The modified Stanton number St_{mod} expresses this ratio. For a modified Stanton number of approximately $St_{mod} > 1.5$, homogeneous mass transfer is no longer possible. In this case, the particles at the inlet are washed out/loaded faster than the particles at the outlet, despite reaching the maximum particle diameter $\tilde{d}_p^{max}$ at the inlet and the minimal particle diameter $\tilde{d}_p^{min}$ at the outlet. Nevertheless, a reduction in the solvent demand $\tilde{V}_{Solvent}$ can still be achieved for $St_{mod} > 1.5$. If the convection is so low that the concentration between the liquid phase and the stationary phase reaches equilibrium at any time and at any point of the column, a gradient of the particle diameter $\tilde{d}_p$ achieves no improvement of objective J_2.

4.3 | Sharp breakthrough curve

The final objective J_3 aims to reach the sharpest breakthrough curve at the outlet of an adsorption column (Case B) as possible. The profile of the particle diameter $\tilde{d}_p$ in axial direction $\tilde{z}$ is displayed in Figure 7 for the homogeneous packing, the five layers by Naidu and Mathews,[10] the optimal solution for J_3, and the optimal five layers. Additionally, Figure 8 shows the breakthrough concentrations $\tilde{c}(\tilde{t},\tilde{z}=1)$ of these four packings and the theoretically optimal sharp curve.

The breakthrough concentration $\tilde{c}(\tilde{t},\tilde{z}=1)$ of the homogeneous packing has the broadest shape (Figure 8). Using a stratified packing,

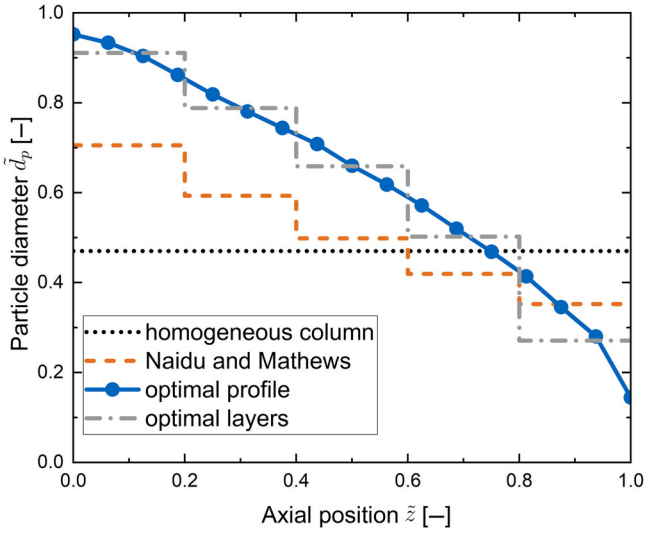

FIGURE 7 Particle diameter $\tilde{d}_p$ as a function of the axial position $\tilde{z}$ for objective J_3 for Case B for the homogeneous column, the five layers by Naidu and Mathews,[10] the optimal profile, and the optimal five layers.

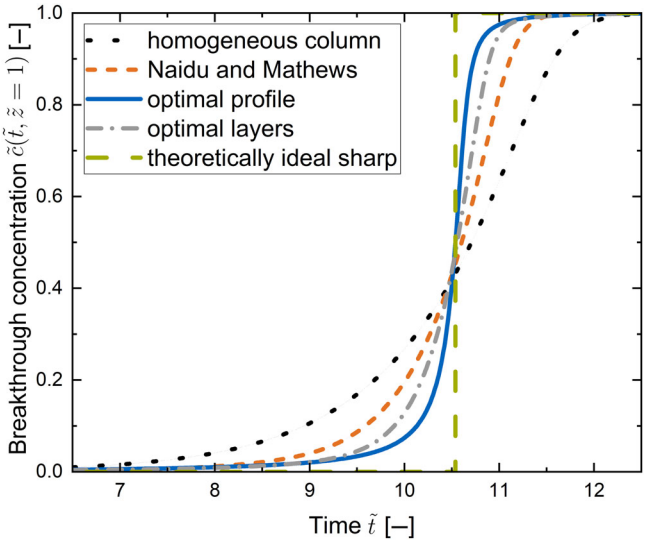

FIGURE 8 Model predicted breakthrough curves of the homogeneous column, the five layers by Naidu and Mathews,[10] the optimal profile, the optimal five layers, and the theoretically perfect sharp curve.

Naidu and Mathews[10] achieved a significantly sharper breakthrough curve than the homogeneous column. The comparison of the predictions of the used model in this work and the experimentally obtained data of Naidu and Mathews[10] are included in the Supplementary Material. Qualitatively, the model predictions and the experimental data are in sufficient agreement. In our model, the five layers by Naidu and Mathews[10] achieve a significantly sharper breakthrough curve (Figure 8). The deviation in terms of the L_2-norm of the difference functions is 42.04% lower than the deviation of the homogeneous packing with equal pressure drop $\Delta\tilde{p}$ (Table 4). Using

TABLE 4 Results of the objective functional J_3 for the homogeneous column, the five layers by Naidu and Mathews,[10] the optimal profile, and the optimal five layers.

Column	J_3
Homogeneous column	1
Naidu and Mathews	0.5796
Optimal profile	0.1966
Optimal layers	0.3744

the optimal control algorithm to optimize the objective functional J_3, we obtain the optimal particle diameter $\tilde{d}_p$ as a function of the axial position $\tilde{z}$ illustrated in Figure 7. The optimal profile of the particle diameter $\tilde{d}_p$ has a more significant gradient along the axial direction $\tilde{z}$ and a decreasing slope. The breakthrough concentration $\tilde{c}(\tilde{t}, \tilde{z} = 1)$ of the optimal packing is the closest to the theoretically optimal sharp curve (Figure 8) and reduces the distance by 80.34% compared to the homogeneous packing (Table 4). The optimal five layers improve the sharpness of the breakthrough curve by 62.56% compared to the homogeneous column (Table 4). Consequently, using the optimal control algorithm, five optimal layers can be determined. This significantly improves the sharpness of the breakthrough curve compared to the layers used in Naidu and Mathews[10] (Figure 8).

Whether stratification reaches improved process performance depends on various factors. For this reason, the methodology presented in this article is particularly valuable to identify whether a stratified packing can provide advantages. If that is the case, optimal profiles of the particle diameter $\tilde{d}_p$ in the axial direction $\tilde{z}$ using optimal control can be determined.

5 | CONCLUSION

In this article, we presented a model-based strategy to design stratified particle packings with varying particle diameter along the axial direction using optimal control. The method was illustrated for the mass transfer from the stationary phase into the liquid phase (Case A) and the mass transfer into the stationary phase from the liquid phase (Case B). An example of Case A is the removal of impurities through washing with a solvent or coffee extraction, and an example of Case B is an adsorption column. Three objective functionals, namely the maximal mass transfer J_1, the minimal solvent demand J_2, and the sharpness of the breakthrough curve J_3 of Case B were investigated. The method effectively optimized mass transfer by determining optimal profiles of the particle diameter as a function of the axial position. Homogeneous packings are optimal for maximizing overall mass transfer. Optimal particle diameter profiles were determined using optimal control to enable homogeneous washing (Case A) or homogeneous loading (Case B). Furthermore, columns with axial gradients of the particle diameter achieved significant savings in solvent demand (up to 32.47%) during washing/loading to a defined target concentration in the stationary phase. In addition, the sharpness of the breakthrough

curve of an adsorption column was improved by 80.34% compared to a homogeneous packing. Moreover, our method can potentially improve the design of stratified particle packings with any varying property in spatial direction for various applications.

Methodologically, future work could include advancing the model to a 2D model by resolving the radial concentration within the porous particles and coupling it with model reduction methods such as proper orthogonal decomposition.[40] Especially for larger particles and slower intra-particle mass transfer, this could increase the model accuracy. A multiscale approach could be considered to describe transport phenomena on a micro-scale level.[26] Naturally, experimental validation of enabling homogeneous mass transfer by stratified particle packings and, thus, reducing the solvent demand to reach a target concentration in the solid phase is highly desirable. The local variation of the concentration in the stationary phase in the axial direction could, for example, be investigated by x-ray micro-computed tomography.[41]

We are convinced that methods like those presented in this contribution will become increasingly important. Various examples of stratified packings have already been shown to have beneficial properties.[9,11–14,17,18,23,42,43] Model-based methods are ideally suited to make optimal use of those benefits.

AUTHOR CONTRIBUTIONS

A. Eppink: Conceptualization (equal); investigation (lead); methodology (equal); visualization (lead); writing – original draft (lead); writing – review and editing (equal). **M. Kuhn:** Conceptualization (equal); funding acquisition (lead); writing – review and editing (supporting). **H. Briesen:** Conceptualization (equal); funding acquisition (lead); methodology (equal); supervision (lead); writing – review and editing (equal).

ACKNOWLEDGMENTS

This work was supported by the DFG, Deutsche Forschungsgemeinschaft. Open Access funding enabled and organized by Projekt DEAL.

CONFLICT OF INTEREST STATEMENT

The authors declare no conflicts of interest.

DATA AVAILABILITY STATEMENT

Figures 1 and 2 contain no numerical data. The numerical data from Figure 3 are only hypothetical to illustrate the optimal control algorithm and tabulated in the provided Supplementary Material Excel file. The numerical data in Figures 4, 5, 6, 7, 8, A.1, and A.2 are simulated results and listed in the Supplementary Material Excel file as well. The experimental data in Figures A.1 and A.2 are taken from Naidu and Mathews[10] and compared with the model predictions in Appendix A.2 in the Supplementary Material. The numerical data of the graphical abstract are the same as in Figure 7 and provided in the Supplementary Material Excel File. The Supplementary Material Excel file also lists the input parameters and numerical results of each case study.

ORCID

A. Eppink https://orcid.org/0009-0007-2640-845X

REFERENCES

1. Dai K, Jiao P, Peng X, et al. Design and optimization of JO-IEX process for highly efficient quaternary separation of 5′-ribonucleotides. *AIChE J*. 2022;68(6):e17592.
2. Jo CY, Kang H-J, Mun S. Improving the performances of a simulated-moving-bed reactor for the synthesis of methyl acetate ester by using partial port-closing strategies. *Chem Eng J*. 2022;435:134887.
3. Guo Y, Jusko V, Xiao G, et al. Separation of $He/N_2/CH_4$ ternary mixtures by a triple-reflux pressure swing adsorption process. *AIChE J*. 2022;68(5):e17569.
4. Zhou J, Wu J, Liu Y, et al. Modeling of breakthrough curves of single and quaternary mixtures of ethanol, glucose, glycerol and acetic acid adsorption onto a microporous hyper-cross-linked resin. *Bioresour Technol*. 2013;143:360-368.
5. Hu G, Xiao G, Guo Y, et al. Separation of methane and nitrogen using ionic liquidic zeolites by pressure vacuum swing adsorption. *AIChE J*. 2022;68(7):e17668.
6. Hargarten VB, Kuhn M, Briesen H. Swelling properties of roasted coffee particles. *J Sci Food Agric*. 2020;100(10):3960-3970.
7. Barroso LA, Macedo AS, Lemos IL, et al. Optimization of the brewing parameters on coffee extraction using a central composite rotatable design. *JSFA Rep*. 2022;2(3):107-115.
8. Noerpel S, Siauw V, Nirschl H. Filter cake washing of mesoporous particles. *Chem Eng Technol*. 2012;35(4):661-667.
9. Pota AA, Mathews AP. Effects of particle stratification on fixed bed absorber performance. *J Environ Eng*. 1999;125(8):705-711.
10. Naidu H, Mathews AP. Acetic acid adsorption dynamics in stratified tapered beds. *Chem Eng J*. 2019;371:337-347.
11. Li M, Liapis AI. Adsorption in a stratified column bed packed with porous particles having partially fractal structures and a distribution of particle diameters. *J Sep Sci*. 2012;35(8):947-956.
12. Sze MFF, McKay G. Enhanced mitigation of para-chlorophenol using stratified activated carbon adsorption columns. *Water Res*. 2012;46(3):700-710.
13. Hernández-Hernández LE, Bonilla-Petriciolet A, Mendoza-Castillo DI, Reynel-Ávila HE. Antagonistic binary adsorption of heavy metals using stratified bone char columns. *J Mol Liq*. 2017;241:334-346.
14. Bruttini R, Liapis AI. The drying rates of spray freeze drying systems increase through the use of stratified packed bed structures. *Int J Heat Mass Transfer*. 2015;90:515-522.
15. Salloum M, Robinson DB. Optimization of flow in additively manufactured porous columns with graded permeability. *AIChE J*. 2022;68(9):e17756.
16. Georgiadis MC, Kostoglou M. On the optimization of drug release from multi-laminated polymer matrix devices. *J Control Release*. 2001;77(3):273-285.
17. Kuhn M, Kirse C, Briesen H. Improving the design of depth filters: a model-based method using optimal control theory. *AIChE J*. 2018;64(1):68-76.
18. Kuhn M, Briesen H. Optimizing the axial resistance profile of submerged hollow fiber membranes. *Processes*. 2021;9(1):20.
19. Ge R, Ghadiri M, Bonakdar T, Hapgood K. 3D printed agglomerates for granule breakage tests. *Powder Technol*. 2017;306:103-112.
20. Neukäufer J, Hanusch F, Kutscherauer M, Rehfeldt S, Klein H, Grützner T. Methodik zur Entwicklung additiv gefertigter Packungsstrukturen im Bereich der thermischen Trenntechnik. *Chem Ing Tech*. 2019;91(7):1014-1023.
21. Kuhn M, Pietsch W, Briesen H. Clarifying thoughts about the clarification of liquids—filtration and the philosophy of science. *Chem Ing Tech*. 2017;89(9):1126-1132.

22. Egidi N, Giacomini J, Maponi P, Perticarini A, Cognigni L, Fioretti L. An advection–diffusion–reaction model for coffee percolation. *Comp Appl Math*. 2022;41(6):229.
23. Li M, Liapis AI. Adsorption in columns packed with porous adsorbent particles having partially fractal structures. *J Sep Sci*. 2013;36(12): 1913-1924.
24. Kuhn M, Briesen H. Dynamic modeling of filter-aid filtration including surface- and depth-filtration effects. *Chem Eng Technol*. 2016;39(3): 425-434.
25. Gu H, Lee DT, Corkery P, et al. Modeling of deposit formation in mesoporous substrates via atomic layer deposition: insights from pore-scale simulation. *AIChE J*. 2022;68(12):e17889.
26. Geerling C, Azimian M, Wiegmann A, Briesen H, Kuhn M. Designing optimally-graded depth filter media using a novel multiscale method. *AICHE J*. 2020;66(2):e16808.
27. Seupel S, Peuker UA. Filterkuchenwäsche makroporöser Kieselgelpartikel. *Chem Ing Tech*. 2019;91(12):1842-1852.
28. Wilkens M, Peuker UA. Grundlagen und aktuelle Entwicklungen der Filterkuchenwaschung. *Chem Ing Tech*. 2012;84(11):1873-1884.
29. Naidu H, Mathews AP. Linear driving force analysis of adsorption dynamics in stratified fixed-bed adsorbers. *Sep Purif Technol*. 2021;257:117955.
30. Sang H, Mao C, Ming F, Xu L, Wei Y, Wu Y. Selective separation and immobilization process of 137Cs from high-level liquid waste based on silicon-based heteropoly salt and natural minerals. *Chem Eng J*. 2022;449:137842.
31. Raji Y, Nadi A, Rouway M, et al. Efficient adsorption of methyl orange on nanoporous carbon from agricultural wastes: characterization, kinetics, thermodynamics, regeneration and adsorption mechanism. *J Compos Sci*. 2022;6(12):385.
32. Schmidt-Traub H, Schulte M, Seidel-Morgenstern A, eds. *Preparative Chromatography*. Wiley-VCH; 2020.
33. Wilson EJ, Geankoplis CJ. Liquid mass transfer at very low Reynolds numbers in packed beds. *Ind Eng Chem Fund*. 1966;5(1):9-14.
34. Mackie JS, Meares P. The diffusion of electrolytes in a cation-exchange resin membrane I. Theoretical. *Proc R Soc Lond A*. 1955; 232(1191):498-509.
35. Chung SF, Wen CY. Longitudinal dispersion of liquid flowing through fixed and fluidized beds. *AIChE J*. 1968;14(6):857-866.
36. Kozeny J. *Über kapillare Leitung des Wassers im Boden: (Aufstieg, Versickerung u. Anwendung auf die Bewässerg); Gedr. mit Unterstützg aus d. Jerome u. Margaret Stonborsugh-Fonds*. Wien: Hölder-Pichler-Tempsky, A.-G. [Abt.] Akad. d. Wiss. 1927.
37. Carman PC. Fluid flow through granular beds. *Trans Inst Chem Eng*. 1937;15:150-166.
38. Vande Wouwer A, Saucez P, Vilas C. *Simulation of ODE/PDE Models with MATLAB®, OCTAVE and SCILAB: Scientific and Engineering Applications*. Springer; 2014.
39. Goh CJ, Teo KL. Control parametrization: a unified approach to optimal control problems with general constraints. *Automatica*. 1988; 24(1):3-18.
40. Pergam P, Briesen H. Reduced order modeling for compressible cake filtration processes using proper orthogonal decomposition. *Comput Chem Eng*. 2023;171:108165.
41. Martinez A, Kuhn M, Briesen H, Hekmat D. Enhancing the x-ray contrast of polymeric biochromatography particles for three-dimensional imaging. *J Chromatogr A*. 2019;1590:65-72.
42. Li M, Liapis AI. The dynamic behavior of a stratified column bed packed with porous adsorbent particles having partially fractal structures and a nonuniform ligand density distribution. *J Sep Sci*. 2012; 35(24):3439-3446.
43. Pota AA, Mathews AP. Adsorption dynamics in a stratified convergent tapered bed. *Chem Eng Sci*. 2000;55(8):1399-1409.

SUPPORTING INFORMATION

Additional supporting information can be found online in the Supporting Information section at the end of this article.

How to cite this article: Eppink A, Kuhn M, Briesen H. Model-based design of stratified packings for enhanced mass transfer using optimal control theory. *AIChE J*. 2024;70(1):e18285. doi:10.1002/aic.18285